CASP1 variants influence subcellular localization, pyroptosome formation and pro-inflammatory cell death in patients with *CASP1*-associated autoinflammatory disease (AID)

Running title: *CASP1* variants influence subcellular localization and pro-inflammatory cell death

Franz Kapplusch[1]*, Felix Schulze[1]*, Sabrina Rabe-Matschewsky[1], Susanne Russ[1], Maik Herbig[2], Michael Christian Heymann[1], Katharina Schoepf[1], Robert Stein[1], Ursula Range[3], Angela Rösen-Wolff[1], Stefan Winkler[1], Christian Michael Hedrich[1,4,5], Jochen Guck[2], Sigrun Ruth Hofmann

[1]Department of Pediatrics, Medizinische Fakultät Carl Gustav Carus, Technische Universität Dresden, Dresden, Germany

[2]Biotechnology Center for Molecular and Cellular Bioengineering, Technische Universität Dresden, Dresden, Germany

[3]Institute for Medical Informatics and Biometry, Medizinische Fakultät Carl Gustav Carus, Technische Universität Dresden, Dresden, Germany

[4]Department of Women's & Children's Health, Institute of Translational Medicine, University of Liverpool, Liverpool, UK.

[5]Department of Paediatric Rheumatology, Alder Hey Children's NHS Foundation Trust Hospital, Liverpool, UK.

*contributed equally

 # Correspondence to:

Sigrun R. Hofmann MD, PhD,

Department of Pediatrics, University Hospital Carl Gustav Carus,

Fetscherstrasse 74,

01307 Dresden, Germany

E-Mail: sigrun.hofmann@uniklinikum-dresden.de

Phone: +49-351-458-6883,

Fax: +49-351-458-4381

Key words

caspase-1, inflammasome, NLRP3, IL-1β, interleukin-1 converting enzyme, apoptosis-associated speck-like protein containing a CARD (ASC), pyroptosome, pyroptosis, speck, gasdermin D

Abstract

Background: *CASP1* variants result in reduced enzymatic activity of procaspase-1 and impaired IL-1β release. Despite this, a subset of carriers develops the clinical picture of systemic autoinflammation. These on the first view contradictory observations can at least partially be explained by increased NF-κB activation through prolonged interaction of variant procaspase-1 with receptor interacting protein kinase (RIP)2. However, little is known about the exact molecular events resulting in pro-inflammatory signaling.

Aim: We aimed to characterize the subcellular localization of variant procaspase-1, their influence on IL-1β release, cell proliferation, phagocytosis and pro-inflammatory cell death (pyroptosis).

Methods: An *in vitro* model for the study of *CASP1* variants was established through shRNA-directed knock-down of endogenous procaspase-1 followed by viral transduction of human monocytes (THP-1) with expression plasmids either encoding wild-type or enzymatically inactive procaspase-1 fusion-reporter proteins. We analyzed subcellular (pro)caspase-1 distribution, inflammasome assembly, and the induction of pyroptosis using fluorescence and confocal microscopy, life-time imaging and Western blot. Proliferation and phagocytosis were assessed using the IncuCyte® live-cell analysis system in combination with pH sensitive probes (e.g. pHrodo E. coli microparticle). Macrophage cell shape changes were investigated by real-time deformability cytometry (RT-DC).

Results: THP-1-derived macrophages carrying *CASP1* variants were characterized by mutation-specific molecular alterations. The p.L265S variant resulted in disturbed nuclear localization of (pro)caspase-1 and reduced formation of cytosolic macromolecular complexes (also called specks or pyroptosomes) after inflammasome stimulation. The p.R240Q variant, as well as an artificial active center mutation of procaspase-1 (p.C285A) promoted speck formation, resulting in increased speck size, which may lead to the amplification of inflammatory signals in response to release of pyroptosomes to the extracellular space. The p.C285A variant additionally mediated impaired inflammatory cell death. Proliferation and phagocytosis of monocytes/macrophages was not influenced by *CASP1* variants investigated, but macrophage deformability was increased after inflammasome stimulation, potentially influencing cell shape changes and migration properties.

Conclusions: Despite reduced enzymatic activity, *CASP1* variants result in pro-inflammatory phenotypes. Besides an increased association/interaction of variant procaspase-1 with RIP2, and therefore enhanced NF-κB activation, we here provide *in vitro* evidence that abnormal pyroptosome formation (p.C285A, p.240Q, p.L265S), impaired nuclear protein localization (p.L265S), reduced pro-inflammatory cell death (p.C285A) and changes in macrophage deformability could contribute to disease pathophysiology of CASP1-AID patients.

Introduction

Naturally occurring variants of the caspase-1 (*CASP1*) gene were recently identified in patients with recurrent fevers and other signs of systemic inflammation [1]. The term *CASP1*-associated autoinflammatory disease (CASP1-AID) has been suggested to characterize this disorder. In most cases, symptoms start in early childhood and include febrile episodes (> 38.5°C) lasting 3 days to 3 weeks, systemic inflammation with C-reactive protein elevation >50 mg/l, and additional complaints, including arthralgia, myalgia and/or exanthema. Some patients exhibit abdominal pain, diarrhea, and lymphadenopathy.

The *CASP1* gene locates to chromosome 11q22.3, comprises 10 exons (NM_033292; NCBI RefSeq [2]) and encodes for procaspase-1. Most of the identified point mutations are located in exon 6, which encodes for the p20 subunit of procaspase-1. Thus, mutations closely localize to the active center of caspase-1 and interfere with hetero-tetramer formation through destabilization of water-mediated hydrogen bonds and hydrophobic interactions at the dimer-dimer interface [1].

Caspase-1 is activated in response to the recognition of pathogen and/or danger associated molecular patterns (PAMPs or DAMPs) through intracellular sensors including NOD-like receptors (NLR). This results in a conformational change allowing for associations with the apoptosis associated speck-like protein containing a CARD (ASC), leading to caspase-1 activation and enzymatic cleavage of pro-interleukin (IL)-1β and pro-IL-18 into their active forms. Furthermore, direct proximity of procaspase-1 molecules results in activation and auto-processing of caspase-1 into the N-terminal caspase recruitment domain (CARD), a central p20 and a C-terminal p10 subunit. The hetero-tetrameric assembly of two p10 and two p20 subunits results in active caspase-1.

The analysis of caspase-1 variants in an *in vitro* cell model (resembling the cellular phenotype of CASP1-AID) revealed variant specific decreased or abrogated enzyme activity and subsequently impaired IL-1β secretion [1]. Whole blood samples of patients confirmed reduced IL-1β secretion, however elevated pro-inflammatory TNF-α levels [1]. The paradox of an inflammatory phenotype in the absence of caspase-1 enzyme activity led to the hypothesis of an upregulation of alternative pro-inflammatory pathways in individuals with *CASP1* variants. Recently, we supported this by demonstrating enhanced NF-κB activation through variant procaspase-1, which is dependent on receptor interacting protein kinase (RIP)2. In the context of CASP1-AID, CARD:CARD interactions between RIP2 and procaspase-1 variants are stabilized which results in increased NF-κB activation [3].

Caspase-1 is not only a key regulator of the innate immune response activating pro-inflammatory cytokines IL-1β and IL-18. It also promotes pyroptosis, an inflammatory form of programmed cell death, by cleaving the pore-forming effector protein gasdermin D (GSDMD) [4]. This leads to plasma membrane pore formation, cell swelling and burst by osmotic lysis and subsequently the release of highly pro-inflammatory cellular components [5, 6]. In this pyroptosis contrasts apoptosis, in which

cellular compartments are condensed and subject to phagocytic uptake of membrane covered apoptotic bodies preventing inflammation.

Pyroptosis is further characterized by the formation of a macromolecular ASC aggregate (ASC speck) preceding cell swelling and cell death. This ASC speck formation has first been described in 1999 in promyelocytic leukemia HL-60 cells, where it was linked to apoptosis [7]. Eight years later, in 2007, Fernandes-Alnemri and colleagues extended this notion by observing cytosolic ASC speck formation in the perinuclear region of immune cells (monocytes) after lipopolysaccharide (LPS) stimulation, subsequently inducing pyroptosis [8]. Therefore, they introduced the term “pyroptosome” for this spherical cytosolic ASC-aggregate/-speck. Recently, the “pyroptosome” polymerization mechanism has been revealed up to a nearly molecular level [9, 10]. After recognition of PAMPs or DAMPs by pyrin domain (PYD) containing receptors like NLRP3 or AIM2, these receptors oligomerize and attract the adapter protein ASC via heterotypic PYD:PYD interaction. The PYD of ASC forms helical filamentous structures (via homotypic PYD:PYD interaction), exposing the CARD of ASC in the periphery. Those CARDs further recruit procaspase-1 via heterotypic CARD:CARD interaction [9, 10] forming a macromolecular speck. Although it is still subject of ongoing discussions, the formation of pyroptosomes and inflammasomes are considered as the same phenomenon [11]. ASC specks serve as activation platforms, recruiting and activating caspase-1.

Of note, speck formation is required for IL-1β processing but not for induction of cell death [12]. Recently, it has been described that pyroptosomes/specks released after cell lysis remained active in the extracellular compartment and kept processing procaspase-1 and pro-IL-1β [13, 14]. In addition, specks were engulfed by macrophages, hence amplifying the inflammatory response within these cells. The *in vivo* relevance of pyroptosome uptake has been highlighted by detecting increased levels of pyroptosomes in the sera of patients with cryopyrin associated periodic syndrome (CAPS), an autoinflammatory disease with gain-of-function mutations within the NLRP3 gene [13].

Additionally, ASC has been suggested to compete with the CARD of RIP2 for binding of procaspase-1 CARD, thereby leading to the down regulation of RIP2-mediated NF-κB activation [15]. Furthermore, ASC is reported to modulate actin polymerization, thus influencing migration of lymphocytes [16]. Finally, ASC activates the transcription of a variety of regulators of apoptosis, proliferation and differentiation, including the initiator caspase-8 and -9, the effector caspase-3, the AP-1 signaling pathways (inducing the pro-inflammatory cytokine IL-8), mitogen-activated protein kinase (MAPK) and NF-κB [17-21].

This study was to investigate the molecular pathophysiology of *loss-of-function* mutations in the *CASP1* gene of patients with CASP1-AID. We provide *in vitro* evidence of the importance of pyroptosome formation and macrophage deformability in the disease pathophysiology of CASP1-AID patients.

Experimental procedures

Plasmids

The plasmid encoding human procaspase-1 was a kind gift from Prof. J. Tschopp (University of Lausanne, Lausanne, Switzerland). The procaspase-1 p.R240Q, p.L265S and p.C285A variants were generated by site directed mutagenesis using the QuickChangeII XL Site-Directed Mutagenesis Kit (Stratagene, La Jolla, CA) following standard protocols. cDNA fragments of wild type procaspase-1 and the variants were cloned into the lentiviral transfer vector p6NST51 or p6NST53 (kindly provided by Prof. Dirk Lindemann, Institute of Virology, University Hospital Carl Gustav Carus, Technische Universität Dresden, Germany) and fused to either mCherry or pEGFP at their N-terminus. The two plasmids p6NST51 and p6NST53 only differed in their resistance for eukaryotic selection and are a variant of p6NST50 [22, 23]. mCherry and EGFP plasmids were purchased from Clontech (Mountain View, CA). All constructs underwent quality control by restriction enzyme digestion and Sanger sequencing.

Antibodies and reagents

The following antibodies were used: anti-IL-1β (H-153), anti–procaspase-1 A-19 (sc-622), anti-caspase-1 p20 C-15 (sc-22163) (all Santa Cruz Biotechnology, Santa Cruz, CA); anti-ASC (AL177; AdipoGen, Epalinges, Schweiz), anti-mCherry (1C51; Abcam, Cambridge, UK), anti-GAPDH (H86045M; Meridian Life Science, Saco, USA), anti-β-Actin (A2228; Sigma-Aldrich, St. Louis, USA), horseradish peroxidase (HRP)-linked anti-rabbit (NA9340; GE Healthcare, Freiburg, Germany), HRP-linked anti-mouse (P0260; DakoCytomation, Glostrup, Denmark), HRP-linked anti-goat (AP186P; Merck Millipore, Billerica, USA), Alexa Fluor 488-linked anti-rabbit (A-11008), Alexa Fluor 488-linked anti-mouse (A-11001) (both Life Technologies, Darmstadt, Germany).

Nigericin and ultra-pure LPS from E. coli O111:B4 were obtained from InvivoGen (Toulouse, France), Ponceau from (Santa Cruz Biotechnology, Santa Cruz, CA). Nuclei in life cell imaging experiments were stained with NucBlue® Live ReadyProbes® Reagent (ThermoFisher Scientific, Schwerte, Germany).

Cell lines and cell culture procedures

The human monocytic cell line THP-1 was originally isolated from a patient with acute monocytic leukemia and is widely used to study immunological processes, e.g. caspase-1 and inflammasome activation [8, 24, 25]. THP-1 cells express inflammasome components such as NLRP1, NLRP3, NLRC4, apoptosis speck like protein containing a CARD (ASC) and caspase-1. After inflammasome stimulation they are able to process and secrete IL-1β. THP-1 monocytic cells usually grow in suspension but can be differentiated to macrophages by adding phorbol-12-myristate-3-acetate (PMA), then adhering to cell surfaces. This stimulation upregulates toll-like receptor 4 (TLR4), which is

necessary for LPS sensing. TLR4 activation by LPS is followed by the upregulation of inflammasome-associated components such as Pro-IL-1β, ASC, NLRP3.

We established an *in vitro* model of a virally transduced human monocytic cell line (THP-1, ATCC TIB-202, LGC Standards GmbH, Wesel, Germany) with shRNA knock-down of endogenous procaspase-1 (a-PCasp1, against the 3'-UTR) reconstituted with either wildtype or variant procaspase-1 fusion-reporter proteins. Briefly, the expression of endogenous procaspase-1 was knocked down using the shRNA expression vector plKO.1 (Addgene, Cambridge, MA). The following target sequences were used: *CASP1*-3'-untranslated region, AAGAGATCCTTCTGTAAAGGT and control, AAGACCTCTTGTTAAGAGAGT. Lentiviral vector particles were produced in HEK293T cells (ATCC, LGC Standards GmbH, Wesel, Germany) transfected with lentiviral transfer plasmids and plasmids psPAX2 and pVSVg. THP-1 cells were transduced with plkO.1 lentiviral stocks and selected with puromycin. Protein knockdown was analyzed by Western blotting. This cell line was then reconstituted with wildtype or variant caspase-1 by transduction of lentiviral vector particles with a multiplicity of infection (MOI) of 0.1 (p6NST51.mCherry.CASP1) or 0.2 (p6NST53.EGFP.CASP1) and selected with zeocin or G418 respectively. THP-1 cells were cultivated in 5% CO_2 at 37°C in RPMI medium 1640 supplemented with 2 mM L-glutamine, 10% fetal calf serum (FCS) and 100 U/ml penicillin and 100 µg/ml streptomycin (all Life Technologies).

HEK 293T cell lines were grown at 37°C in humidified atmosphere of air with 5% CO2 in DMEM supplemented with 2 mM L-glutamine, 10% FCS and penicillin/ streptomycin.

Image processing and quantification of pyroptosome formation

Pyroptosome formation in THP-1 cells was analyzed by immunofluorescence analysis of mCherry/EGFP caspase-1 specks. THP-1 cells were cultured in 0.7 cm^2 chambers (8-well Lab-Tek chambered coverglass system; ThermoFisher Scientific), stimulated as described, stained with NucBlue® Live ReadyProbes® Reagent (ThermoFisher Scientific, Schwerte, Germany) and subsequently imaged using a Zeiss Axiovert 200M microscope (Carl Zeiss Microscopy GmbH, Germany) and a Zeiss Plan-Apochromat 10x/0.45NA objective and reflectors for Hoechst staining (EX 340-380 nm, EM 435-485 nm), GFP (EX 465-495 nm, EM 500-540nm) and cherry (EX 530-560 nm, EM 590-650 nm). A CCD Coolsnap HQ camera (Photometrics, USA) and Visiview/MetaMorph (Visitron Systems GmbH, Puchheim, Germany) software was used for data acquisition. Live cell imaging was conducted in RPMI (ThermoFisher Scientific) at 37°C and 5% CO_2 at the light microscopy facility BIOTEC/CRTD.

Image processing was carried out with ImageJ/Fiji software [26](http://imagej.nih.gov/ij/; http://fiji.sc/Fiji). Specks/pyroptosomes were counted manually in the mCherry- or GFP-channel, total cell numbers were determined by quantification of nuclei in the Hoechst channel. Speck intensity was measured as the maximum intensity of each speck. For analysis of the speck diameter, the full-width at half-maximum intensity was applied.

Protein expression analysis

Caspase-1 was measured in serum-free cell supernatants or cell lysates by SDS PAGE, using caspase-1 polyclonal Ab (sc-514; Santa Cruz, CA), and IL-1β polyclonal Ab (AF-401-NA; R&D Systems, Minneapolis, MN). Cells were lysed and processed as reported previously [3, 15]. Cell lysates were analyzed by sodium dodecyl sulfate polyacrylamide gel electrophoresis (SDS-PAGE), subjected to Western blotting, and immunochemical detection using the respective antibodies.

Measurement of secreted IL-1β

Concentrations of mature IL-1β in the supernatant were determined using *cytometric bead arrays* (CBA) from Becton Dickinson (Franklin Lakes, NJ).

Immunoblotting of precipitated supernatant was performed by adding an equal volume of methanol and 0.25 volumes of chloroform followed by centrifugation for 3 min at 20,000 g. The upper phase was discarded, the same volume of methanol added and centrifuged for 3 min at 20,000 g. The precipitate was dried and taken up in LDS-sample buffer containing reducing agent (Invitrogen), denatured for 10 min at 95°C and separated by Bis-Tris denaturing SDS-PAGE. Proteins were blotted onto 0.2 mM nitrocellulose membranes, blocked in 3% milk and incubated with indicated primary and corresponding secondary antibodies. Chemiluminescent signals were recorded with a CCD-camera and respective images contrast-enhanced in a linear fashion.

Assessment of cell death

Cells were cultured in serum-free RPMI with 1% ITS-G, L-glutamine and penicillin/streptomycin and stimulated as indicated. Cells treated with 0.1% TritonX-100 were used as death positive control. LDH-release into supernatant was determined with the Cytotoxicity Detection Kit PLUS (Roche Applied Science, Mannheim, Germany) following manufacturer's instructions.

Immunofluorescence staining, Confocal and fluorescence microscopy

THP-1 cells were incubated on collagen coated culture slides (BioCoat 8-Well Collagen Culture Slide, BD 354630) and differentiated with 2.5 ng/ml PMA overnight, primed and stimulated as indicated and fixed in 4% paraformaldehyde (Sigma-Aldrich, St. Louis, MO) for 15 min at room temperature, washed and permeabilized in PBS containing 0.04% saponin (Sigma-Aldrich, St. Louis, MO) and 1% BSA (Sigma-Aldrich, St. Louis, MO) for 1 h. Next, cells were stained with appropriate primary antibodies for 1 h, followed by staining with fluorochrome-labeled secondary antibodies for 45 min. Cover slips were mounted on glass slides in 4′,6-Diamidin-2-phenylindol (DAPI) containing Vectashield mounting medium from Vector Laboratories (Burlingame, CA). Slides were subjected to imaging on an inverted Zeiss LSM 510 confocal microscope (Carl Zeiss, Jena, Germany) with a 40× or 63 × 1.4NA objective lens or on an inverted Leica TCS SP5 microscope (Leica Microsystems,

Wetzlar, Germany) using a Leica HC PL APO 40x/0.7NA. An argon laser was used for excitation of Alexa Fluor 488 at wavelengths of 488 nm, whereas a helium-neon laser (543 nm) was used for excitation of mCherry, and a Laser Diode (405 nm) for the excitation of Hoechst or DAPI.

Cell viability assay (Alamar Blue)

Cell viability was assessed using Alamar Blue Cell Viability Assay (DAL1100, Life Technologies, Grand Island, USA) by following the manufacturer's instructions. 2.5 x 10^5 THP-1 cells were seeded in 24-well plates with 500 µl RPMI Medium 1640 supplemented with 2 mM L-glutamine, 10% fetal calf serum, 100 U/ml penicillin, 100 µg/ml streptomycin (all Life Technologies) and primed with 2.5 ng/ml PMA overnight. After 24 h 50 µl Alamar Blue reagent was added to the cell culture medium. Fluorescence signals were measured at 570/600 nm (excitation/emission) on the microplate reader Infinite M200 (Tecan).

Cell cycle analysis

For cell cycle analysis 2 x 10^5 THP-1 cells/ 6-well were synchronized by serum starvation. After four days the cell cycle was restarted (RPMI 1640 media with 10 % FCS) and the cells cultured for additional four days. Cells were collected, resuspended in PBS and permeabilized by adding drop-wise ice-cold ethanol (to a final concentration of 70%), incubated for 1 h at 4°C. Samples were centrifuged at 400×g for 5 minutes, resuspended in PBS containing 50 µg/ml propidium iodide (PI) plus 50 µg/ml RNase A and incubated for 30 minutes at 37°C protected from light. Thereafter, cells were analyzed of PI fluorescence on a LSRII flow cytometer (BD Biosciences).

Cell proliferation assay

Cell proliferation was assayed using an IncuCyte® ZOOM Live-Cell Analysis System (Essen BioScience, Ann Arbor, MI, USA), by collecting real-time data of cell confluence. Cells were seeded on 96-well plates (4,000 cells/well) and analyzed over 40 hours. Cell confluence was monitored and data were obtained by analyzing the cell confluence increment over time using the IncuCyte S2 software and expressed as percentage relative to time point 0. Experiments were conducted with three replicates for each experimental condition, two to four image fields per well and repeated at least three times.

Phagocytosis assay

Phagocytosis was assayed using an IncuCyte® ZOOM Live-Cell Analysis System (Essen BioScience, Ann Arbor, MI, USA). Cells were seeded on 96-well plates (4,000 cells/well), treated with 2.5 ng/ml PMA for 24 hours. pHrodo™ Green E. coli BioParticles® were added, and the increase of green fluorescence was analyzed by scanning the plate and acquiring fluorescent and phase-contrast images in real time. Two to three images per well from three technical replicates were taken every 20 min for

4 hours using a 20x objective lens. Images were analyzed using the IncuCyte® Basic Software and expressed as percentage of green object confluence increase relative to time point 0. Green channel acquisition time was 400 ms. Cell segmentation was achieved by applying a mask in order to exclude cells from background. An area filter was applied to exclude objects below 50 μm^2. Green channel background noise was subtracted with the Top-Hat method of background non-uniformity correction. Fluorescence signal was quantified applying a mask.

Real-time deformability cytometry (RT-DC)

RT-DC in combination with a custom-made image analysis algorithm allows determination of properties of single cells such as cell size, contour and deformation in real-time [27]. In brief, THP-1 cells with a shRNA knockdown of endogenous procaspase-1 and re-constitution of procaspase-1 wildtype or variants were differentiated to macrophages with PMA (2.5 ng/ml) over night and primed with LPS (2 µg/ml) for 3 h. Cells were centrifuged at 300 xg for 10 min and resuspended in PBS (2 x 10^6 cells/300 µl) without magnesium and calcium with 0.5% methylcellulose (36718 Methyl cellulose, viscosity 4000 cPs , Alfa Aesar). Cells were stimulated with 5 µM nigericin directly before measuring. The cell suspension was flowed through a microfluidic channel constriction of 30 µm width at a flow rate of 0.16 µl/s and measured for 45 min every 3 min. Every single cell was illuminated with an LED and imaged with a camera. After background subtraction, the contour is determined in real-time and cells are computed in real-time. Inertia ratio and volume of the cell were also calculated based on the contour, as described in [28]. In brief, the inertia ratio origins from the second moment of area, and is the ratio of elongation in flow direction and orthogonal to it. Volume of cells is computed by a mathematical rotation of the contour around the axis defined by the centroid of the cell and the flow direction [28]. The algorithms to obtain inertia ratio and volume as well as all other analysis tool for RT-DC data are available through the open source software ShapeOut 0.8.8. (available at https://github.com/ZELLMECHANIK-DRESDEN/ShapeOut).

Statistics

Statistical analysis was performed using GraphPad Prism and SPSS software. Statistical analysis for IL-1β secretion (out of 7 independent experiments) was examined using two-way Anova and multiple comparison test adjusted by Bonferroni. The statistical significance for the cumulative numbers of specks (out of 4 independent experiments) was determined using two-way Anova and multiple comparison test adjusted by Bonferroni. The statistical analysis for speck diameters was performed using one-way Anova with Sidiak's multiple comparison test. P-values are indicated by *, $p < 0.05$; **, $p < 0.01$; *** $p < 0.001$; ****, $p < 0.0001$, or n.s. = not significant.

Results

Generation of genetically modified human monocyte cell lines expressing variant procaspase-1

To investigate whether *CASP1* variants p.R240Q, p.L265S and p.C285A [1] influence proliferation, phagocytosis, and cell death of human monocytes/macrophages, we generated and established an *in vitro* model of a virally transduced human monocytic cell lines (THP-1). Initially, we induced shRNA-mediated knock-down of endogenous procaspase-1 (THP-1/a-PCasp1, down to ~20%) and then reconstituted caspase-1 expression with plasmids either encoding for wild-type (WT) or variant procaspase-1 (p.R240Q, p.L265S and an artificial p.C285A variant with an active center mutation, **Fig. 1A,B and Suppl. Fig. 1A,B**) linked or not linked to fusion-reporter proteins. Transduction efficiency was tested by fluorescence-based flow cytometry analysis (data not shown), Western blotting (**Fig. 1A and Suppl. Fig. 1A,B**) and quantitative RT-PCR (**Fig. 1C**). Despite comparable mRNA expression between cell lines generated and despite using different multiplicity of infection (MOI), protein expression differed repeatedly between lines, showing higher protein levels for the WT fusion reporter protein when compared to all of the procaspase-1 variants. Of note, almost comparable protein expression levels were achieved between tagged and untagged cell lines with a MOI of 0.06. However, the p.L265S variant showed repeatedly lower expression levels (**Fig. 1A**). Thus, "untagged" cell lines served as controls for further experiments with the fusion-reporter protein transduced THP-1/a-PCasp1 cells.

To determine cell proliferation, cell health and viability of all cell lines generated, we used the real-time quantitative live cell imaging IncuCyte® platform (Essen Bioscience) and quantified cell confluence over time. As shown in **Suppl. Fig. 1C**, cell proliferation was not affected by fluorescent tags and did not show differences for the analyzed procaspase-1 variants when compared to wildtype cells.

The biological functionality of the new THP-1 monocyte model was further evaluated mimicking bacterial infection with LPS priming and stimulation with either nigericin or ATP as an activator of the NLRP3 inflammasome. IL-1β secretion, measured by cytometric bead array (CBA) (**Fig. 1D**) and Western blot analysis of cell culture supernatants (**Fig. 1E**), was used as readout for caspase-1 activation. In response to LPS and nigericin, cells expressing WT procaspase-1 (GFP-WT) secreted significantly more mature IL-1β as compared to GFP control cells or the inactive procaspase-1 variant p.C285A, and slightly more than the naturally occurring variants p.L265S, and p.R240Q (**Fig. 1D**). Consistent with these observations, we were able to detect the mature form of IL-1β by Western blotting in the supernatant of cell lines challenged under the same conditions (**Fig. 1E**).

Procaspase-1 variants influence pyroptosome formation

A characteristic sign of inflammasome activation within a single cell is the formation of a perinuclear ASC speck, which can also be referred to as pyroptosome [5, 8] or even as inflammasome [11], containing multimerized sensor (e.g. NLRP3), adaptor (ASC), and effector (caspase-1) proteins. We

previously demonstrated in murine cells that procaspase-1 and the enzymatically inactive p.C284A variant are recruited to the pyroptosome [29]. Therefore, we performed experiments to determine whether human monocyte cell lines bearing procaspase-1 variants p.R240Q, p.L265S and p.C285A exhibit speck formation in response to inflammasome activation, and if speck formation differs between variants.

Assuming that the monocyte cell model generated sufficiently reproduces physiological macrophage functions *in vitro* and is not affected by fluorescent tags (**see Fig. 1 and Suppl. Fig. 1**), we conducted live cell imaging experiments with THP-1/a-PCasp1 cells reconstituted with either WT or variant procaspase-1 fusion-reporter proteins. THP-1 monocytes were differentiated to macrophages overnight using 2.5 ng/ml phorbol 12-myristate 13-acetate (PMA). In response to stimulation with LPS alone, cells did not show remarkable changes (data not shown). After priming with LPS followed by the addition of nigericin GFP-WT and variant procaspase-1 cell lines (GFP-C285A, GFP-L265S, and GFP-R240Q) formed one cytosolic macromolecular speck after approximately 45-60 min, which remained for more than 5 hours (**Fig. 2A,B**). Consistent with previous data [29], the p.C285A variant formed a bigger and significantly brighter speck when compared to WT cells. Remarkably, procaspase-1 p.L265S resulted in significantly decreased speck numbers and reduced signal intensity. Speck number and intensity in the p.R240Q variant were comparable to those in WT but showed increased speck size.

Next, we tested whether GFP-WT or GFP-L265S specks had resolved before detection by microscopy contributing to the differences observed regarding speck numbers at time point 310 min (**Fig. 2A**). We analyzed speck numbers on images acquired from a time-series (over 6 hours after NLRP3 stimulation with nigericin at 10 min intervals). The number of newly formed specks were added to speck number on previous slides at each time point, gaining a cumulative speck number (**Fig. 2B,C**). Differences (**Fig. 2A**) were confirmed with significantly decreased number of specks/pyroptosomes in procaspase-1 variants p.C285A and p.L265S when compared to WT and p.R240Q at the time points 240, 300 and 360 min.

Interestingly, speck sizes did not associate with enzyme activity of procaspase-1 variants. To quantify speck sizes, we used the “mean of half maximum intensity” method and analyzed the fluorescence microscopy images, which have been acquired for the experiments in **Fig. 2A-C** and determined a mean procaspase-1 speck diameter of 1.21 µm (SD ± 0.336) in GFP-WT cells, 1.44 µm (SD ± 0.496) in GFP-C285A cells, 1.12 µm (SD ± 0.361) in GFP-L265S cells and 1.44 µm (SD ± 0.517) in GFP-R240Q cells. Specks of GFP-C285A and GFP-R240Q cells were significantly larger when compared to GFP-WT specks. Specks in GFP-L265S cells were smaller than those in GFP-WT cells which, however, did not reach statistical significance (p=0.07) (**Fig. 2D**). Therefore we performed higher resolution imaging using a confocal microscope. As shown in **Fig. 2E**, specks for the procaspase-1 p.L265S variant were significantly smaller than WT specks.

Using life cell fluorescence microscopy imaging, we noticed differences in speck intensities between cell lines (**Fig. 2A**). Measuring speck intensities over time, we observed procaspase-1 specks fading in GFP-WT cells almost immediately after their formation (within 20 min) (**Fig. 2F**). GFP-R240Q specks remained slightly brighter and fading occurred slower (within 40 min), and signal intensities remained at a higher level when compared to GFP-WT. Specks in GFP-L265S cells only reached a signal intensity that was around 2/3 of that in GFP-WT cells, which faded within 20 min (almost to the background before pyroptosome formation) (**Fig. 2F**, -10 min time point). In contrast, GFP-C285A specks remained more stable and showed significantly slower fading. Differences were quantified at time points 100 min and 200 min (**Fig. 2G**) demonstrating significantly brighter specks in GFP-C285A and significantly dimmer specks in GFP-L265S when compared to GFP-WT cells.

As previously demonstrated [29], within the same cell, WT caspase-1 specks decrease more rapidly in fluorescence intensity when compared to ASC stained specks, suggesting caspase-1 auto-processing as a possible explanation. Here, we also demonstrate rapid speck fading and decreased speck intensity in cells expressing variant procaspase-1 p.L265S, which lacks enzymatic activity [1]. Assuming that p.L265S is not capable of auto-processing, we wondered about dynamics and distribution of caspase-1 subunits. We stained stimulated THP-1/a-PCasp1 cells reconstituted with either mCherry (Ch) or the fluorescent fusion proteins Ch-WT or Ch-L265S (all with comparable protein expression, **Suppl. Fig. 1B**) with antibodies directed against CARD, the p10 or p20 subunit of caspase-1 (**Fig. 3A**). Both in Ch-WT and Ch-L265S cells, specks co-localized with CARD, p10 and p20. Thus, we concluded that mCherry signals represent the localization of procaspase-1 within speck, as has been previously demonstrated by our group for the murine p.C284A variant [29]. Furthermore, in Ch-WT and Ch-L265S cells, procaspase-1 specks co-localize with ASC after NLRP3 stimulation (**Fig. 3A**). Interestingly, in contrast to reduced numbers of caspase-1 specks in Ch-L265S cells when compared to Ch-WT monocytes, all cell lines (Ch-WT, Ch-L265S, Ch) generated the same amount of ASC-specks (**Fig. 3B**).

Furthermore, in both cell lines, Ch-WT and Ch-L265S, nigericin stimulation resulted not only in speck formation but also in pyroptosis, shown by an increase in cell volume, the presence of cell membrane vesicles, and a decrease in intracellular mCherry fluorescence intensity due to the release of plasma membrane vesicles (**Suppl. Fig. 1D+E**).

Variant procaspase-1 p.L265S results in disturbed subcellular localization

To study subcellular localization of procaspase-1 in macrophages, we performed life cell confocal laser scanning microscopy of PMA-differentiated THP-1 monocytes, showing cytoplasmic and nuclear localization of the mCherry signal in WT cells (**Fig. 3C,D**). Interestingly, Ch-WT cells, in which functional caspase-1 can self-process, exhibited predominantly nuclear localization of the CARD domain and the p10 subunit, but not of the p20 subunit. Cells with the enzymatically attenuated

procaspase-1 variant p.L265S (Ch-L265S) almost exclusively exhibited caspase-1 localization in the cytoplasm (**Fig. 3C,D**).

To exclude the possibility that subcellular distribution of fusion reporter proteins differs from endogenous procaspase-1 localization, we performed antibody staining of endogenous procaspase-1 using native THP-1 and a-PCasp1 cells (**Suppl. Fig. 2A**). Corresponding to results in Ch-WT cells, we observed slightly increased fluorescent signal for CARD in the nucleus. In contrast, p20 and p10 subunits distributed almost equally between the nucleus and the cytoplasm. We did not observe differences between a-PCasp1 (knockdown of endogenous procaspase-1 to ~20%) and native THP-1 cells indicating that antibody staining is very sensitive and detects small amounts of endogenous protein.

Since antibody staining against the procaspase-1 subunits did not allow to distinguish between the endogenous and transduced fluorescent reporter fusion protein, we performed experiments in HEK293T cells, which lack endogenous procaspase-1 and pro-IL-1β. We transfected HEK293T cells with Ch, Ch-WT and Ch-L265S together with pro-IL-1β expression plasmids. Western blot analysis showed comparable protein expression, and CBA assays the expected IL-1β secretion in Ch-WT but not in Ch-L265S cells (data not shown). Using confocal laser scanning microscopy, we detected primarily cytoplasmic localization of the p.L265S variant, which was also shown by antibody staining of the caspase-1 subunits CARD, p20 and p10 (**Suppl. Fig. 2B**).

Taken together, these results demonstrate that the fluorescent reporter attached to CARD does not influence subcellular distribution of procaspase-1 variants. Macrophages with variant procaspase-1 p.L265S, however, exhibit disturbed nuclear localization of caspase-1 when compared to cells expressing wild-type caspase-1.

Procaspase-1 variants do not influence phagocytic capacity of macrophages

One major functions of monocytes and macrophages is the phagocytosis of pathogens. To address the question of whether procaspase-1 variants influence phagocytosis, we used the real-time quantitative live cell imaging IncuCyte® platform (Essen BioScience) and analyzed the different cell lines for the capacity to phagocytose pHrodo® Green E. coli BioParticles®. Of note, phagocytosis between the cell lines varied insignificantly (**Fig. 4**).

Procaspase-1 variants influence Gasdermin D processing and pyroptosis

Knowing that procaspase-1 variants influence speck formation and IL-1β maturation and therefore the canonical inflammasome pathway, we investigated their influence on gasdermin-mediated programmed cell death, pyoptosis. Gasdermin D (GSDMD) is a substrate of caspase-1 and caspase-11/4/5. It induces pore formation in the plasma membrane of monocytes/macrophages through its N-terminal fragment, which oligomerizes and inserts in the plasma membrane giving rise to rapid cell lysis. The C-terminal part of GSDMD has inhibitory function and protects from pyroptosis [4, 30].

THP-1/a-PCasp1 cells either bearing WT procaspase-1 or variants were differentiated to macrophages using PMA, followed by priming with LPS and stimulation with nigericin to induce inflammasome assembly. Activation of WT procaspase-1 through the canonical inflammasome pathway led to GSDMD cleavage and the release of its N-terminal fragment, whereas enzymatically attenuated procaspase-1 variants showed abrogated (p.C285A) or decreased (p.L265S, p.R240Q) GSDMD cleavage (**Fig. 5A**).

Furthermore, after priming with LPS, the addition of nigericin resulted in a significant increase of lactate dehydrogenase (LDH) release into supernatants of WT transduced cells, which was used as a measure of cell death (**Fig. 5B**). Procaspase-1 variants also showed an increased LDH release after nigericin stimulation, which, however, was lower when compared to WT cells.

Procaspase-1 variants influence the deformability of macrophages after inflammasome stimulation

Since migration of macrophages into tissues requires their activation and cell deformation, we tested whether procaspase-1 variants influence morphological properties of cells. THP-1/a-PCasp1 cells bearing WT or variant procaspase-1 were differentiated to macrophages using PMA, primed with LPS and stimulated with nigericin. Using the recently developed technique of real time deformability cytometry (RT-DC), macrophages were deformed in a microfluidic channel constriction of 30 µm, and mechanical and morphological cell parameters were measured in real-time [27, 31]. The inertia ratio, a parameter that quantifies deformation, and cell volumes were determined at 0 min and 20 min of treatment. The measured cell volume was not significantly different between WT and procaspase-1 variant cell lines (GFP-WT, GFP-240, GFP-265, GFP-285) (**Fig. 6A**). The inertia ratio was significantly different at 0 min comparing GFP-WT versus GFP-L265S ($p=0.04764$) cells. 20 min after nigericin stimulation the inertia ratio, as a measure of deformation, showed significant differences between GFP-WT and GFP-L265S ($p=0.04827$) and also between GFP-WT and GFP-C285A ($p=0.01188$) indicating a higher deformation of the procaspase-1 variants compared to WT (**Fig. 6A-C**).

Discussion

We recently showed that *CASP1* variants [1, 32] that cause an autoinflammatory disease (CASP1-AID) exhibit increased interaction with RIP2, thereby leading to enhanced activation of the pro-inflammatory transcription factor NF-κB. This, in turn may contribute to uncontrolled engagement of inflammatory signaling pathways [3]. Since *CASP1* mutations can also occur in asymptomatic family members and, at low frequencies, in the healthy normal population, many questions remain. We hypothesized that usually heterozygous *CASP1* variants represent a disease-modifying factor in the context of other mechanisms that contribute to the expression of CASP1-AID. In this study, we focused on the effects of two disease-associated *CASP1* variants (p.L265S, p.R240Q) and a described

missense mutation in the active center of procaspase-1 (p.C285A) on inflammasome/pyroptosome formation, cell proliferation, phagocytic function and mechanical properties of macrophages.

In the past, ASC speck formation was considered essential for IL-1β activation and release but not for pyroptosis [12]. Recently, however, we linked loss of (pro)caspase-1 activity to increased pyroptosome/speck formation in murine cells [29]. Reduced or absent enzyme activity stabilized the pyroptosome in murine macrophages and resulted in increased speck sizes, intensity and prolonged speck persistence, thus promoting interactions between ASC and procaspase-1 molecules in the pyroptosome. This was independent of the vital state of cells and could occur in the extracellular space after cell lysis. Furthermore, we suggested that pro-inflammatory signal transmission through spreading of specks during cell division may be an additional mechanism amplifying inflammation [29].

In the here described system of THP-1/a-PCasp1 cells, reconstitution with either WT or variant procaspase-1, priming with LPS and stimulation of NLRP3 inflammasome assembly with nigericin or ATP resulted in IL-1β release that was proportional to the residual enzymatic activity of procaspase-1 variants. The formation of perinuclear specks/pyroptosomes was differentially influenced by individual procaspase-1 variants regarding the number, size and fluorescence intensity of specks and did not correlate with the residual enzymatic activity. Variants p.C285A (an artificial active center mutation) and p.R240Q (occurring as hetero- and homozygous mutation in patients) showed increased pyroptosome sizes and fluorescence intensity, which was comparable to previous findings in the murine p.C284A variant [29]. In contrast, the p.L265S procaspase-1 variant (heterozygous mutation in patients) associated with significantly reduced pyroptosome formation when compared to WT caspase-1, with smaller procaspase-1 specks and reduced fluorescence, while the size of the ASC specks did not differ. Assuming that the p.L265S variant is not subject to auto-processing [1], we detected all procaspase-1 subunits inside the specks by antibody staining for CARD, p20 and p10. Confirming our previous data from the murine system [29], we detected all three procaspase-1 subunits inside the WT specks, co-localizing with ASC. Reduced speck formation in cells carrying the p.L265S variant may be explained by protein misfolding [1]. This, in combination with the absence of enzymatic activity in this variant (lack of auto-processing), may also contribute to disturbed subcellular localization (“nuclear exclusion”). Observed differences in speck formation, which do not associate with residual enzyme activity of tested procaspase-1 variants, suggest that further mechanisms exist that contribute to the pro-inflammatory phenotype in CASP1-AID patients.

One of the major biological functions of monocytes and macrophages is their capacity as phagocytes. Thus, we analyzed the phagocytic ability of mutant p.R240Q, p.L265S and p.C285A *CASP1* cell lines

in response to PAMPs. The capacity to phagocytose pHrodo® Green E. coli BioParticles was not different between WT and the analyzed procaspase-1 variants.

Since cytomechanical properties of cells correlate very closely with physiological and pathological changes in cell function, the measurement of cell mechanics as a biophysical characterization method of cytoskeletal changes has been established in recent years [33]. The relatively new method of real-time deformability cytometry (RT-DC) allows the characterization of cell alterations associated with remodeling processes. It has been shown that efficient reorganization of the actin cytoskeleton is required for rapid ASC speck formation [34, 35]. Therefore, impaired speck formation by *CASP1* variants should lead to changes in cytoskeleton compliance. Using RT-DC we analyzed the influence of procaspase-1 variants on cell mechanics and found that *CASP1* variants associate with higher cell deformability. As macrophage migration into tissues requires activation and mechanical deformation, one could speculate that a higher deformation of cells bearing procaspase-1 variants could facilitate the migration of macrophages. In contrast to our results, Ekpenyong and colleagues [33] reported increased cell rigidity of murine macrophages (BMDM) associated with S. typhimurium infection and therefore inflammation. The diverse results could be due to the use of different cell lines (human monocytic cells, THP-1 versus BMDM), stimulations (LPS and nigericin versus S. typhimurium infection) and techniques (RT-DC versus digital holographic microscopy, DHM). Further projects following this hypothesis are warranted and will analyze the exact influences of procaspase-1 variants on cell deformability and migration.

Conclusions

Procaspase-1 variants contribute to the inflammatory phenotype in patients with CASP1-AID despite decreased IL-1β release. In addition to previously reported increased interactions between procaspase-1 variants and RIP2 [3], stabilization of ASC-pyroptosomes, and pyroptosome spreading during cell division [29], enzymatically attenuated human procaspase-1 variants do not prevent macrophages from pyroptosome formation, but influence the number, size and intensity of pyroptosomes independent of the residual enzymatic activity of caspase-1. Furthermore, human procaspase-1 variants do not influence cell proliferation and phagocytic capacity, however, lead to increased macrophage deformability, which could facilitate cell migration into inflamed tissue. Data from this study provide new insights into the involvement of caspase-1 in monocyte/macrophage biology and effects of reduced enzyme activity. Further investigations are needed to elucidate the exact molecular effects of *CASP1* variants and modifying genetic and/or environmental factors causing CASP1-AID in some but not other individuals affected.

Acknowledgments

Images were generated at the Biopolis Dresden Imaging Platform (BioDIP) including the Biotechnology Center of the TU Dresden (BIOTEC), the Center for Regenerative Therapies (CRTD), and the Core Facility Cellular Imaging (CFCI). The authors thank especially Hella Hartmann (BioDIP/BIOTEC), and Silke Tulok and Anja Walter (CFCI) for excellent support. We thank Prof. Dirk Lindemann (Dresden, Germany) for kindly providing plasmids. The work was supported by the German Research Foundation (DFG-KFO249, HO4510/1-2 to S.R.H., and RO/471-11 to A.R.W. and S.W.), the Else Kröner Fresenius Stiftung (Else-Kröner-Promotionskolleg, EKFS foundation to S.R-M.), and the Roland Ernst Stiftung für Gesundheitswesen (3/17 to S.R.H).

Conflicts of interest

The authors declare no conflict of interests.

Author contributions

FK, SRa and FS conducted most of the experiments and analysed the results. SRu conducted experiments on the IL-1β secretion of cells and constructed vectors for expression of fluorescently labelled proteins. MH performed the RT-DC data analysis. CMH, SW, JG, RS and ARW helped with interpretation of data and revised the manuscript. SRH designed the study, conducted some of the *in vivo* live cell imaging experiments and the IncuCyte experiments, analysed data and wrote the paper. All authors reviewed the results and approved the final version of the manuscript.

Figures

Figure 1. Generation and characterization of human monocytic cell lines with procaspase-1 knock-down and expression of fluorophore-tagged procaspase-1 variants. Fusion proteins of the green fluorophore (EGFP) tagged to either WT procaspase-1 (WT) or enzymatic inactive (p.C285A) or attenuated (p.L265S, p.R240Q) procaspase-1 variants were expressed in THP-1 cells with knock-down of the endogenous procaspase-1 (a-PCasp1). EGFP alone served as control. Caspase-1 activation was induced by priming with 1 µg/ml LPS for 3 h, followed by 10 µM nigericin or 2 mM ATP for 1 h. **A**, THP-1 cells were lentivirally transduced with shRNA against the 3'-UTR region of the procaspase-1 mRNA. The Western blot analysis shows a highly efficient knock-down of procaspase-1 expression (a-PCasp1) with a reduction of protein levels down to ~20%. Protein level of procaspase-1 fusion protein (PCasp1, 74 kDa), partially degraded caspase-1 (60 kDa) and endogenous or untagged procaspase-1 (~50 kDa) are shown by Western blotting with a caspase-1 CARD-detecting antibody (anti-Caspase-1 (scA-19)) and densitometric analysis (quantification of caspase-1 expression compared to β-Actin, which served as a loading control). Slightly different protein expression of variant procaspase-1 fusion-reporter proteins compared to WT remained despite repeated re-generation of cell lines with different MOIs. **B,** Schematic drawing of procaspase-1 WT and variants is shown. The fluorescent protein (EGFP) was fused to the N-terminal CARD of procaspase-1. The analyzed mutations localize to the p20 subunit of procaspase-1. **C,** Caspase-1 expression of a-PCasp1 cell lines reconstituted with WT or variant procaspase-1 measured by qRT-PCR. The relative mRNA expression was calculated as fold-increase compared to three reference genes (*GAPDH*/*ALAS1*/*B2M*). **D+E,** *IL-1β release* into supernatants was measured by cytometric bead array (D) and Western blot analysis (E). Cells expressing WT procaspase-1 (GFP-WT) secreted significantly more mature IL-1β compared to the inactive procaspase-1 variant p.C285A and GFP control when treated with both LPS and nigericin. IL-1β is displayed as fold increase compared to unstimulated GFP-WT cells. **A,E**, Data are representative of three independent experiments. **C,D**, Experiments are displayed as the mean ± SD. ns, not stimulated; WT, wildtype; scr, scramble shRNA; empty, reconstitution performed with empty vector; Sup, supernatant; ** $p<0.01$

Figure 2. Enzymatically attenuated procaspase-1 variants do not prevent macrophages from pyroptosome formation but influences its number, size and intensity. Fusion proteins of EGFP tagged to either WT procaspase-1 (WT) or enzymatic inactive or attenuated (p.C285A, p.L265S, p.R240Q) procaspase-1 variants were expressed in THP-1 cells with knock-down of the endogenous procaspase-1 (a-PCasp1). EGFP alone served as control. Cells were differentiated with 2.5 ng/ml phorbol 12-myristate 13-acetate (PMA) to macrophages overnight. Caspase-1 activation was induced by priming with 1 µg/ml LPS for 3 h, followed by 10 µM nigericin and analysed by life-cell imaging. **A**, Representative fluorescence microscopy images of GFP-procaspase-1 specks at time point 310 min after the addition of nigericin are shown. Arrowheads indicate cells that formed specks. **B**, Life-time

images of the fluorescence channel were aquired every 10 min over a time period of 400 min. At each time point, specks emerging for the first time were counted and added to the number of specks in previous slides. Specks were counted and related to the total amount of nuclei (Hoechst stains) within the same field. Between 700-1000 cells per cell line were analysed for speck formation. Results of two independent experiments are shown, which are representative for a total of 4 independent experiments. **C**, GFP-procaspase-1 specks, that were observed by fluorescence microscopy after 60, 120, 180, 240, 300 and 360 min (B) were counted and related to the total amount of nuclei (Hoechst stains). Cumulative numbers of specks out of 4 independent experiments are shown. Statistical significance was determined using two-way Anova and multiple comparison test adjusted by Bonferroni. **D,** Speck size/diameter in cells expressing GFP-WT or GFP-tagged procaspase-1 variants was measured from fluorescence microscopy images (n=70 specks/cell line out of 4 independent experiments; one-way Anova with Sidiak's multiple comparison test). **E,** Speck size in cells expressing Ch-WT or Ch-tagged procaspase-1 variant p.L265S was measured from confocal images (n=20 specks/cell line out of 5 independent experiments; unpaired t-test, mean ± SD). **F**, As demonstrated in A, specks of the procaspase-1 variant cell lines show differences in their intensity. Graphs indicate mean values of maximum fluorescence intensities of GFP-WT or GFP-tagged procaspase-1 variant specks. First speck formation was set as the starting point (0 min) and assessed for each pyroptosome individually. Intensity levels 10 min before speck formation (-10 min) represent the background signal from the cytosol. Speck intensities after 100 and 200 min were chosen for statistical analysis in **G** (n=22/each time point).

Figure 3: Variant procaspase-1 p.L265S formed smaller pyroptosomes compared to wildtype, and all procaspase-1 subunits are part of the pyroptosome. A, Representative fluorescence microscopy images of THP-1 cells with knock-down of the endogenous procaspase-1 (a-PCasp1) reconstituted with Cherry (Ch)-WT or Ch-L265S (red channel). Cells were differentiated with 2.5 ng/ml phorbol 12-myristate 13-acetate (PMA) to macrophages overnight. Caspase-1 activation was induced by priming with 1 µg/ml LPS for 3 h, followed by 20 µM nigericin for 1 h. Then, cells were washed and stained with an antibody targeting ASC or the CARD, p20 or p10 subunit of caspase-1, followed by staining with an Alexa^{488} secondary antibody (green channel). The overlay of the red and green channel is shown as Merge. Nuclei were stained with Hoechst (blue channel). Ch-WT and Ch-L265S co-localized with CARD, p10 and p20 in all pyroptosomes (Merge), whereas Ch control cells did not show pyroptosome formation in the red channel, however some pyroptosomes in the green channel, corresponding to the residual endogenous procaspase-1 after shRNA knockdown or to endogenous ASC. **B,** Quantification of speck positive cells compared to the total cell number of the image (n=700 cells/cell line out of 4 independent experiments; mean ± SD). Interestingly, in contrast to diminished numbers of Ch-L265S specks compared to Ch-WT, all cell lines (Ch-WT, Ch-L265S, Ch) generated the same amount of the ASC-specks. **C+D, Macrophages with variant procaspase-1**

p.L265S showed disturbed nuclear localization compared to wildtype. Representative confocal microscopy images of THP-1 cells with knock-down of the endogenous procaspase-1 (a-PCasp1) reconstituted with Ch, Ch-WT or Ch-L265S (red channel). Cells were differentiated with 2.5 ng/ml phorbol 12-myristate 13-acetate (PMA) to macrophages overnight. Cells were stained with antibodies targeting the CARD, p20 or p10 subunit of caspase-1, followed by staining with an Alexa^{488} secondary antibody (green channel). The overlay of the red and green channel is shown as Merge. Nuclei were stained with Hoechst (blue channel). The enzymatically attenuated procaspase-1 variant p.L265S (Ch-L265S) almost exclusively localized to the cytoplasm when fused to mCherry at their N-terminus.

Figure 4: Procaspase-1 variants do not influence pHrodo® Green E. coli Bioparticles® phagocytosis of THP1 macrophages. A+B, THP-1 cells with knock-down of the endogenous procaspase-1 (a-PCasp1) reconstituted with WT and procaspase-1 variants (A, mCherry fusion proteins or B, "untagged") were differentiated with 2.5 ng/ml phorbol 12-myristate 13-acetate (PMA) to macrophages overnight. Using the real-time quantitative live cell imaging IncuCyte® platform (Essen BioScience) cell lines were analyzed side-by-side under the same conditions for their capacity to phagocytose pHrodo® Green E. coli BioParticles®, which only fluoresce when localized in the acidic environment of phagolysosomes. Aquired images were quantified for green object confluence (%) for each time point over 4 hours. Image analysis and fluorescence quantification were performed with the IncuCyte® Basic Software. **C,** Representative images of fluorescence object quantification are shown at time point 0, 1 and 2 hours.

Figure 5: Procaspase-1 variants influence Gasdermin D processing and therefore pyroptosis. A, THP-1/a-PCasp1 cells bearing procaspase-1 WT or variants were differentiated to macrophages with PMA, LPS-primed and stimulated with nigericin. The activation of WT procaspase-1 led to GSDMD cleavage and the release of its N-terminal fragment (p30), whereas enzymatically attenuated procaspase-1 variants show abrogated (p.C285A) or decreased (p.L265S, p.R240Q) GSDMD cleavage. A representative Western blot analysis is displayed. **B,** After LPS priming the addition of nigericin resulted in a significant increase of lactate dehydrogenase (LDH) release into supernatants of WT transduced cells, representing cell death (n=4). Procaspase-1 variants also showed an increased LDH release after nigericin stimulation, which was however less compared to WT.

Figure 6: Morphological and mechanical properties of macrophages analyzed by real-time deformability cytometry (RT-DC). Representative scatter and contour plots (A) and statistical analysis (B) of inertia ratio, indicating increased inertia ration of GFP-285 and GFP-265 compared to GFP-WT. THP-1 cells were differentiated to macrophages with PMA (2.5 ng/ml, 16 h), LPS-primed (1 µg/ml, 3 h) and stimulated with nigericin. The inertia ratio as well as the volume (cell size) was determined for measurements taken at 0 min and 20 min of treatment. The cell volume was not

significantly different for any of the states (GFP-WT, GFP-240, GFP-265, GFP-285) at any time point. The inertia ratio (I) is a parameter that quantifies deformation (I=1 means circle, higher I means more deformed). Linear mixed models analysis was performed to obtain statistical significance. Analyses have been performed using ShapeOut 0.8.8, *, $p<0.05$.

Supplementary Figure 1. Generation and characterization of human monocytic cell lines with procaspase-1 knock-down and expression of mCherry-tagged and "untagged" procaspase-1 variants. A, Representative Western blot analysis of THP-1 cells with knock-down of the endogenous procaspase-1 (a-PCasp1) and reconstitution with either "untagged", "Flag-tagged" or fusion proteins of the red fluorophore (mCherry) tagged to either WT procaspase-1 (WT) or procaspase-1 variants are shown. mCherry, Empty vector, scr and THP-1 nativ served as controls. **B,** Western blot analysis shows a highly efficient knock-down of procaspase-1 expression (a-PCasp1) with a reduction of protein levels down to ~20%. Protein level of procaspase-1 fusion protein (PCasp1, 74 kDa), partially degraded caspase-1 (60 kDa) and endogenous or untagged procaspase-1 (~50 kDa) are shown by Western blotting with a caspase-1 CARD-detecting antibody (anti-Caspase-1 (scA-19)) and densitometric analysis (quantification of caspase-1 expression compared to β-Actin, which served as a loading control). **C,** Cell proliferation of all generated cell lines was examined side-by-side under the same conditions by using the real-time quantitative live cell imaging IncuCyte® platform. The aquired phase contrast images were quantified for cell confluence over time. Cell proliferation was not affected by fluorescent tags and did not show differences for the analyzed procaspase-1 variants compared to WT cells (n=4). **D,** THP-1/a-PCasp1 reconstituted with Ch-WT or Ch-L265S were differentiated to macrophages with PMA, LPS-primed and stimulated with nigericin (as described above). Life-time imaging was performed and representative confocal microscopy images of both cell lines are shown (fluorescence channel). Nigericin stimulation resulted not only in speck formation but also in pyroptosis shown by an increase in cell volume, the occurrence of cell membrane vesicles, and a decrease in intracellular mCherry fluorescence intensity. Specks are marked with yellow arrowheads, scale = 20 μm. **E**, Quantitative fluorescence intensity analysis, showing the decrease of the mCherry fluorescence signal over time. After 80 sec, the unstimulated cell (ns) showed still more than 80% of the fluorescence intensity of its initial value (cell marked with white arrow). In contrast, nigericin stimulation led to a significant decrease of fluorescence intensity (down to 45% after 80 sec). The visible cell swelling after 120 sec results in a massive cytoplasmic outflow (and therefore loss of mCherry signal, white arrow), which is marked by the kink in the fluorescence intensity curve. After 210 sec, almost no fluorescence signal of the cell was detectable. Quantification was done by using CellProfiler 2.0 software. AU, arbitrary units; scale = 20 μm.

Supplementary Figure 2. A, Subcellular localization of procaspase-1 domains in native THP-1 and THP-1/a-PC1 cells. Cells were differentiated for 24 hours with PMA to macrophages and stained

with antibodies against the CARD (anti-caspase-1, sc A-19), the p20 (anti-caspase-1 p20, sc C-15) and the p10 subunit (anti-caspase-1 p10, sc C-20) of procaspase-1 followed by secondary staining with Alexa Fluor^{488} (green channel). Nuclei (Nc) were stained with NucBlue Fixed Ready Probes Reagent (blue channel). The merge displays the overlay of the blue and green channel. Representative confocal fluorescence images are shown. Scale = 20 μm; BF, bright field. **B, Subcellular localization of procaspase-1 domains in transfected HEK293T cells.** HEK293T cells were transfected with expression plasmids for Ch, Ch-WT and the *CASP1* variant p.L265S (Ch-265). In addition, pro-interleukin-1β (Pro-IL-1β) was co-transfected. Cells were fixed and stained with antibodies against the CARD domain, the p20 and the p10 subunit of procaspase-1 as mentioned above (green channel). mCherry fused WT and variant procaspase-1 are displayed in the red channel. The merge displays the overlay of the red and green channel. Representative confocal fluorescence images are shown. Scale = 20 μm.

References

[1] H. Luksch, M.J. Romanowski, O. Chara, V. Tüngler, E.R. Caffarena, M.C. Heymann, P. Lohse, I. Aksentijevich, E.F. Remmers, S. Flecks, N. Quoos, J. Gramatté, C. Petzold, S.R. Hofmann, S. Winkler, F. Pessler, T. Kallinich, G. Ganser, A. Nimtz-Talaska, U. Baumann, V. Runde, B. Grimbacher, J. Birmelin, M. Gahr, J. Roesler, A. Rösen-Wolff, Naturally Occurring Genetic Variants of Human Caspase-1 Differ Considerably in Structure and the Ability to Activate Interleukin-1β, Human Mutation, 34 (2013) 122–131.

[2] K.D. Pruitt, T. Tatusova, G.R. Brown, D.R. Maglott, NCBI Reference Sequences (RefSeq): current status, new features and genome annotation policy, Nucleic Acids Res, 40 (2012) D130-135.

[3] M.C. Heymann, S. Winkler, H. Luksch, S. Flecks, M. Franke, S. Russ, S. Ozen, E. Yilmaz, C. Klein, T. Kallinich, D. Lindemann, S. Brenner, G. Ganser, J. Roesler, A. Rosen-Wolff, S.R. Hofmann, Human procaspase-1 variants with decreased enzymatic activity are associated with febrile episodes and may contribute to inflammation via RIP2 and NF-kappaB signaling, J Immunol, 192 (2014) 4379-4385.

[4] J. Shi, Y. Zhao, K. Wang, X. Shi, Y. Wang, H. Huang, Y. Zhuang, T. Cai, F. Wang, F. Shao, Cleavage of GSDMD by inflammatory caspases determines pyroptotic cell death, Nature, (2015).

[5] T. Bergsbaken, S.L. Fink, B.T. Cookson, Pyroptosis: host cell death and inflammation, Nat Rev Microbiol, 7 (2009) 99-109.

[6] S. Ruhl, K. Shkarina, B. Demarco, R. Heilig, J.C. Santos, P. Broz, ESCRT-dependent membrane repair negatively regulates pyroptosis downstream of GSDMD activation, Science, 362 (2018) 956-960.

[7] J. Masumoto, S. Taniguchi, K. Ayukawa, H. Sarvotham, T. Kishino, N. Niikawa, E. Hidaka, T. Katsuyama, T. Higuchi, J. Sagara, ASC, a novel 22-kDa protein, aggregates during apoptosis of human promyelocytic leukemia HL-60 cells, The Journal of biological chemistry, 274 (1999) 33835–33838.

[8] T. Fernandes-Alnemri, J. Wu, J.-W. Yu, P. Datta, B. Miller, W. Jankowski, S. Rosenberg, J. Zhang, E.S. Alnemri, The pyroptosome: a supramolecular assembly of ASC dimers mediating inflammatory cell death via caspase-1 activation, Cell death and differentiation, 14 (2007) 1590–1604.

[9] K. Kersse, M. Lamkanfi, M.J.M. Bertrand, T. Vanden Berghe, P. Vandenabeele, Interaction patches of procaspase-1 caspase recruitment domains (CARDs) are differently involved in procaspase-1 activation and receptor-interacting protein 2 (RIP2)-dependent nuclear factor κB signaling, The Journal of biological chemistry, 286 (2011) 35874–35882.

[10] A. Lu, V.G. Magupalli, J. Ruan, Q. Yin, M.K. Atianand, M.R. Vos, G.F. Schröder, K.A. Fitzgerald, H. Wu, E.H. Egelman, Unified polymerization mechanism for the assembly of ASC-dependent inflammasomes, Cell, 156 (2014) 1193–1206.

[11] P. Broz, V.M. Dixit, Inflammasomes: mechanism of assembly, regulation and signalling, Nat Rev Immunol, (2016).

[12] M.S. Dick, L. Sborgi, S. Ruhl, S. Hiller, P. Broz, ASC filament formation serves as a signal amplification mechanism for inflammasomes, Nat Commun, 7 (2016) 11929.

[13] A. Baroja-Mazo, F. Martín-Sánchez, A.I. Gomez, C.M. Martínez, J. Amores-Iniesta, V. Compan, M. Barberà-Cremades, J. Yagüe, E. Ruiz-Ortiz, J. Antón, S. Buján, I. Couillin, D. Brough, J.I. Arostegui, P. Pelegrín, The NLRP3 inflammasome is released as a particulate danger signal that amplifies the inflammatory response, Nature immunology, 15 (2014) 738–748.

[14] B.S. Franklin, L. Bossaller, D.d. Nardo, J.M. Ratter, A. Stutz, G. Engels, C. Brenker, M. Nordhoff, S.R. Mirandola, A. Al-Amoudi, M.S. Mangan, S. Zimmer, B.G. Monks, M. Fricke, R.E. Schmidt, T. Espevik, B. Jones, A.G. Jarnicki, P.M. Hansbro, P. Busto, A. Marshak-Rothstein, S. Hornemann, A. Aguzzi, W. Kastenmüller, E. Latz, The adaptor ASC has extracellular and 'prionoid' activities that propagate inflammation, Nature immunology, 15 (2014) 727–737.

[15] A. Sarkar, M. Duncan, J. Hart, E. Hertlein, D.C. Guttridge, M.D. Wewers, ASC Directs NF- B Activation by Regulating Receptor Interacting Protein-2 (RIP2) Caspase-1 Interactions, The Journal of immunology, 176 (2006) 4979–4986.

[16] S.K. Ippagunta, R.K.S. Malireddi, P.J. Shaw, G.A. Neale, L. Vande Walle, D.R. Green, Y. Fukui, M. Lamkanfi, T.-D. Kanneganti, The inflammasome adaptor ASC regulates the function of adaptive

immune cells by controlling Dock2-mediated Rac activation and actin polymerization, Nature immunology, 12 (2011) 1010–1016.
[17] B.B. McConnell, P.M. Vertino, Activation of a caspase-9-mediated apoptotic pathway by subcellular redistribution of the novel caspase recruitment domain protein TMS1, Cancer Res, 60 (2000) 6243-6247.
[18] J. Masumoto, T.A. Dowds, P. Schaner, F.F. Chen, Y. Ogura, M. Li, L. Zhu, T. Katsuyama, J. Sagara, S.i. Taniguchi, D.L. Gumucio, G. Núñez, N. Inohara, ASC is an activating adaptor for NF-κB and caspase-8-dependent apoptosis, Biochemical and Biophysical Research Communications, 303 (2003) 69–73.
[19] M. Molmeret, S.D. Zink, L. Han, A. Abu-Zant, R. Asari, D.M. Bitar, Y. Abu Kwaik, Activation of caspase-3 by the Dot/Icm virulence system is essential for arrested biogenesis of the Legionella-containing phagosome, Cell Microbiol, 6 (2004) 33-48.
[20] M. Hasegawa, R. Imamura, K. Motani, T. Nishiuchi, N. Matsumoto, T. Kinoshita, T. Suda, Mechanism and repertoire of ASC-mediated gene expression, J Immunol, 182 (2009) 7655-7662.
[21] D.J. Taxman, E.A. Holley-Guthrie, M.T.-H. Huang, C.B. Moore, D.T. Bergstralh, I.C. Allen, Y. Lei, D. Gris, J.P.-Y. Ting, The NLR adaptor ASC/PYCARD regulates DUSP10, mitogen-activated protein kinase (MAPK), and chemokine induction independent of the inflammasome, The Journal of biological chemistry, 286 (2011) 19605–19616.
[22] D.A. Amer, G. Kretzschmar, N. Muller, N. Stanke, D. Lindemann, G. Vollmer, Activation of transgenic estrogen receptor-beta by selected phytoestrogens in a stably transduced rat serotonergic cell line, J Steroid Biochem.Mol Biol, 120 (2010) 208-217.
[23] M.C. Heymann, S. Rabe, S. Ruß, F. Kapplusch, F. Schulze, R. Stein, S. Winkler, C.M. Hedrich, A. Rösen-Wolff, S.R. Hofmann, Fluorescent tags influence the enzymatic activity and subcellular localization of procaspase-1, Clinical immunology (Orlando, Fla.), 160 (2015) 172–179.
[24] F. Martinon, K. Burns, J. Tschopp, The inflammasome: a molecular platform triggering activation of inflammatory caspases and processing of proIL-beta, Mol Cell, 10 (2002) 417-426.
[25] V. Petrilli, S. Papin, C. Dostert, A. Mayor, F. Martinon, J. Tschopp, Activation of the NALP3 inflammasome is triggered by low intracellular potassium concentration, Cell Death.Differ., 14 (2007) 1583-1589.
[26] J. Schindelin, I. Arganda-Carreras, E. Frise, V. Kaynig, M. Longair, T. Pietzsch, S. Preibisch, C. Rueden, S. Saalfeld, B. Schmid, J.Y. Tinevez, D.J. White, V. Hartenstein, K. Eliceiri, P. Tomancak, A. Cardona, Fiji: an open-source platform for biological-image analysis, Nat Methods, 9 (2012) 676-682.
[27] O. Otto, P. Rosendahl, A. Mietke, S. Golfier, C. Herold, D. Klaue, S. Girardo, S. Pagliara, A. Ekpenyong, A. Jacobi, M. Wobus, N. Topfner, U.F. Keyser, J. Mansfeld, E. Fischer-Friedrich, J. Guck, Real-time deformability cytometry: on-the-fly cell mechanical phenotyping, Nat Methods, 12 (2015) 199-202, 194 p following 202.
[28] M. Herbig, A. Mietke, P. Muller, O. Otto, Statistics for real-time deformability cytometry: Clustering, dimensionality reduction, and significance testing, Biomicrofluidics, 12 (2018) 042214.
[29] R. Stein, F. Kapplusch, M.C. Heymann, S. Russ, W. Staroske, C.M. Hedrich, A. Rosen-Wolff, S.R. Hofmann, Enzymatically inactive procaspase-1 stabilizes the ASC-pyroptosome and supports pyroptosome spreading during cell division, J Biol Chem, (2016).
[30] N. Kayagaki, I.B. Stowe, B.L. Lee, K. O'Rourke, K. Anderson, S. Warming, T. Cuellar, B. Haley, M. Roose-Girma, Q.T. Phung, P.S. Liu, J.R. Lill, H. Li, J. Wu, S. Kummerfeld, J. Zhang, W.P. Lee, S.J. Snipas, G.S. Salvesen, L.X. Morris, L. Fitzgerald, Y. Zhang, E.M. Bertram, C.C. Goodnow, V.M. Dixit, Caspase-11 cleaves gasdermin D for non-canonical inflammasome signalling, Nature, 526 (2015) 666–671.
[31] O. Otto, P. Rosendahl, S. Golfier, A. Mietke, M. Herbig, A. Jacobi, N. Topfner, C. Herold, D. Klaue, S. Girardo, M. Winzi, E. Fischer-Friedrich, J. Guck, Real-time deformability cytometry as a label-free indicator of cell function, Conf Proc IEEE Eng Med Biol Soc, 2015 (2015) 1861-1864.
[32] H. Luksch, S. Winkler, M.C. Heymann, F. Schulze, S.R. Hofmann, J. Roesler, A. Rosen-Wolff, Current knowledge on procaspase-1 variants with reduced or abrogated enzymatic activity in autoinflammatory disease, Curr Rheumatol Rep, 17 (2015) 45.
[33] A.E. Ekpenyong, S.M. Man, S. Achouri, C.E. Bryant, J. Guck, K.J. Chalut, Bacterial infection of macrophages induces decrease in refractive index, J Biophotonics, 6 (2013) 393-397.

[34] S.M. Man, L.J. Hopkins, E. Nugent, S. Cox, I.M. Glück, P. Tourlomousis, J.A. Wright, P. Cicuta, T.P. Monie, C.E. Bryant, Inflammasome activation causes dual recruitment of NLRC4 and NLRP3 to the same macromolecular complex, Proceedings of the National Academy of Sciences of the United States of America, 111 (2014) 7403–7408.
[35] S.M. Man, A. Ekpenyong, P. Tourlomousis, S. Achouri, E. Cammarota, K. Hughes, A. Rizzo, G. Ng, J.A. Wright, P. Cicuta, J.R. Guck, C.E. Bryant, Actin polymerization as a key innate immune effector mechanism to control Salmonella infection, Proc Natl Acad Sci U S A, 111 (2014) 17588-17593.

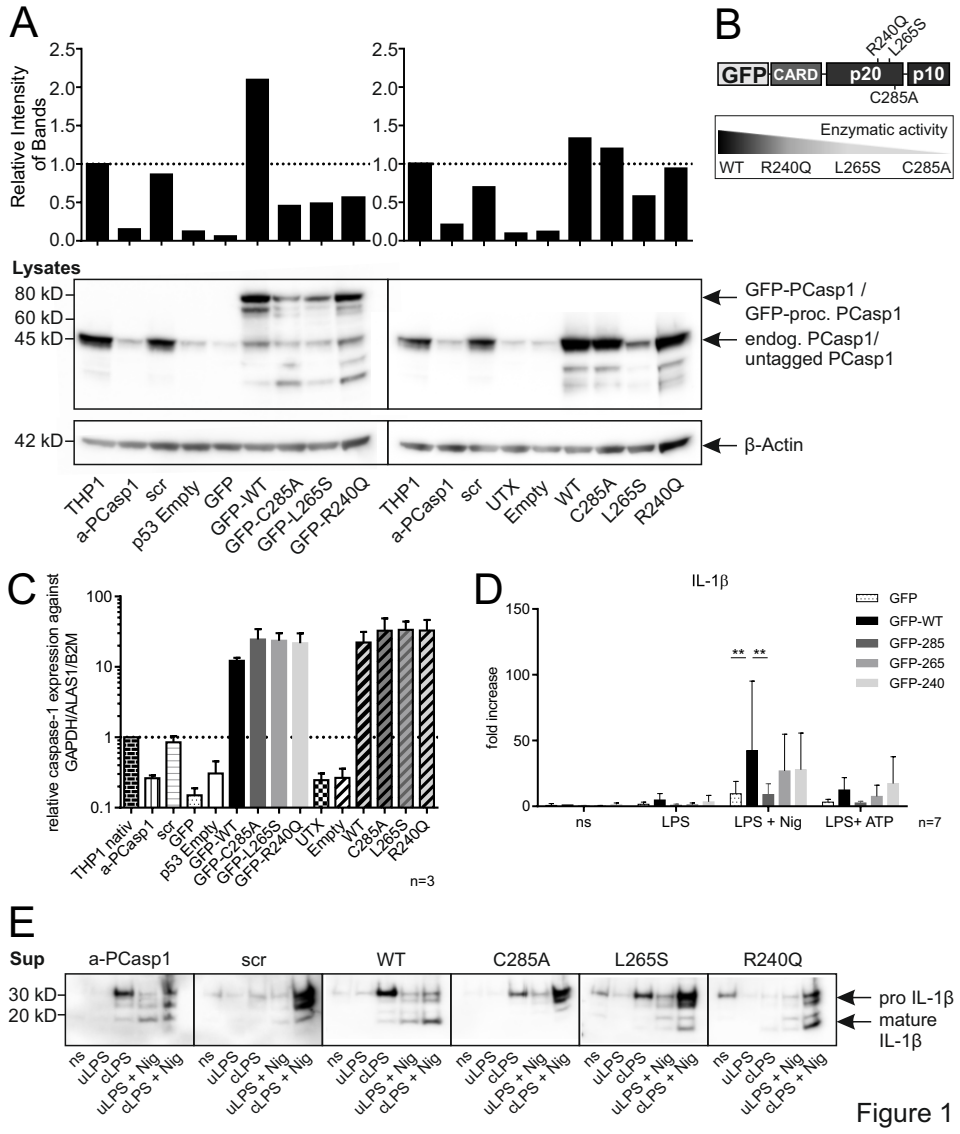
A
Relative Intensity of Bands
2.5
2.0
1.5
1.0
0.5
0.0
B
R240Q
L265S
GFP
CARD
p20
p10
C285A
Enzymatic activity
WT
R240Q
L265S
C285A
Lysates
80 kD
60 kD
45 kD
GFP-PCasp1 /
GFP-proc. PCasp1
endog. PCasp1/
untagged PCasp1
42 kD
β-Actin
THP1
a-PCasp1
scr
p53 Empty
GFP
GFP-WT
GFP-C285A
GFP-L265S
GFP-R240Q
THP1
a-PCasp1
scr
UTX
Empty
WT
C285A
L265S
R240Q
C
relative caspase-1 expression against GAPDH/ALAS1/B2M
100
10
1
0.1
THP1 nativ
a-PCasp1
scr
GFP
p53 Empty
Empty
GFP-WT
GFP-C285A
GFP-L265S
GFP-R240Q
UTX
Empty
WT
C285A
L265S
R240Q
n=3
D
IL-1β
fold increase
150
100
50
0
GFP
GFP-WT
GFP-285
GFP-265
GFP-240
**
**
ns
LPS
LPS + Nig
LPS+ ATP
n=7
E
Sup
a-PCasp1
scr
WT
C285A
L265S
R240Q
30 kD
20 kD
pro IL-1β
mature
IL-1β
ns
uLPS
cLPS
uLPS + Nig
cLPS + Nig

Figure 1

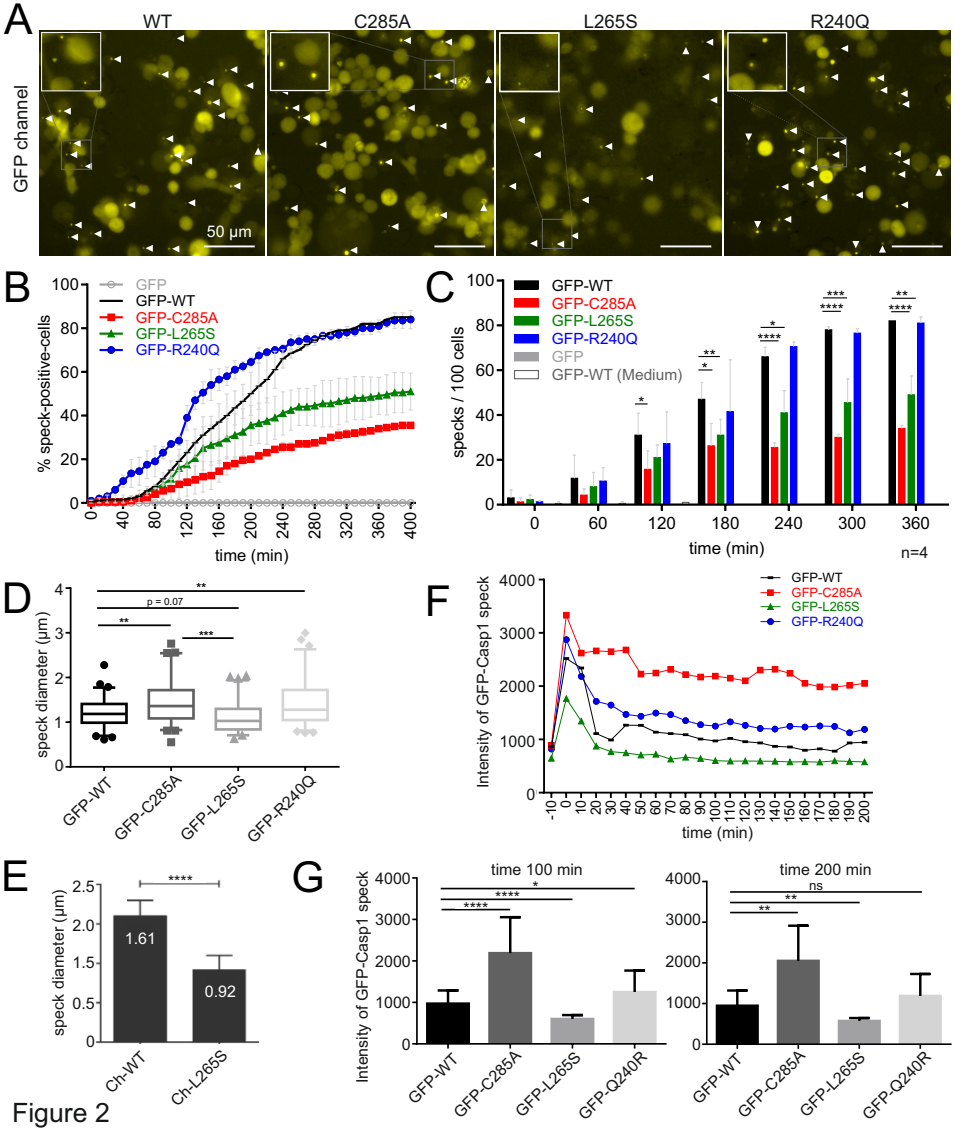
A
WT
C285A
L265S
R240Q
GFP channel
50 µm
B
GFP
GFP-WT
GFP-C285A
GFP-L265S
GFP-R240Q
% speck-positive-cells
time (min)
C
GFP-WT
GFP-C285A
GFP-L265S
GFP-R240Q
GFP
GFP-WT (Medium)
specks / 100 cells
time (min)
n=4
D
p = 0.07
speck diameter (µm)
GFP-WT
GFP-C285A
GFP-L265S
GFP-R240Q
F
GFP-WT
GFP-C285A
GFP-L265S
GFP-R240Q
Intensity of GFP-Casp1 speck
time (min)
E
speck diameter (µm)
1.61
0.92
Ch-WT
Ch-L265S
G
time 100 min
time 200 min
ns
Intensity of GFP-Casp1 speck
GFP-WT
GFP-C285A
GFP-L265S
GFP-Q240R

Figure 2

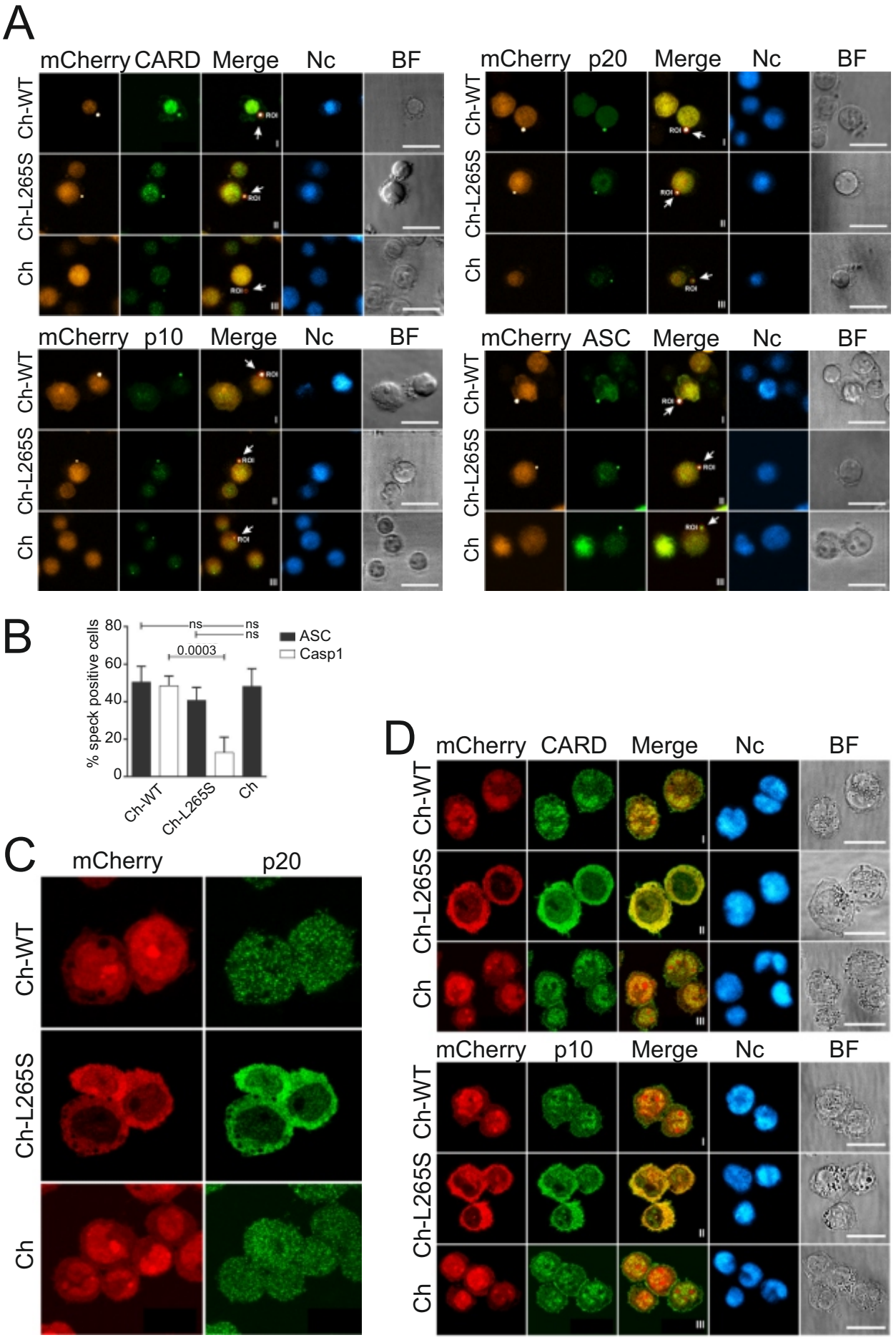
A
mCherry CARD Merge Nc BF
mCherry p20 Merge Nc BF
mCherry p10 Merge Nc BF
mCherry ASC Merge Nc BF
Ch-WT
Ch-L265S
Ch
ROI
B
% speck positive cells
80
60
40
20
0
ns
ns
ns
0.0003
ASC
Casp1
Ch-WT
Ch-L265S
Ch
C
mCherry
p20
Ch-WT
Ch-L265S
Ch
D
mCherry CARD Merge Nc BF
mCherry p10 Merge Nc BF
Ch-WT
Ch-L265S
Ch

Figure 3

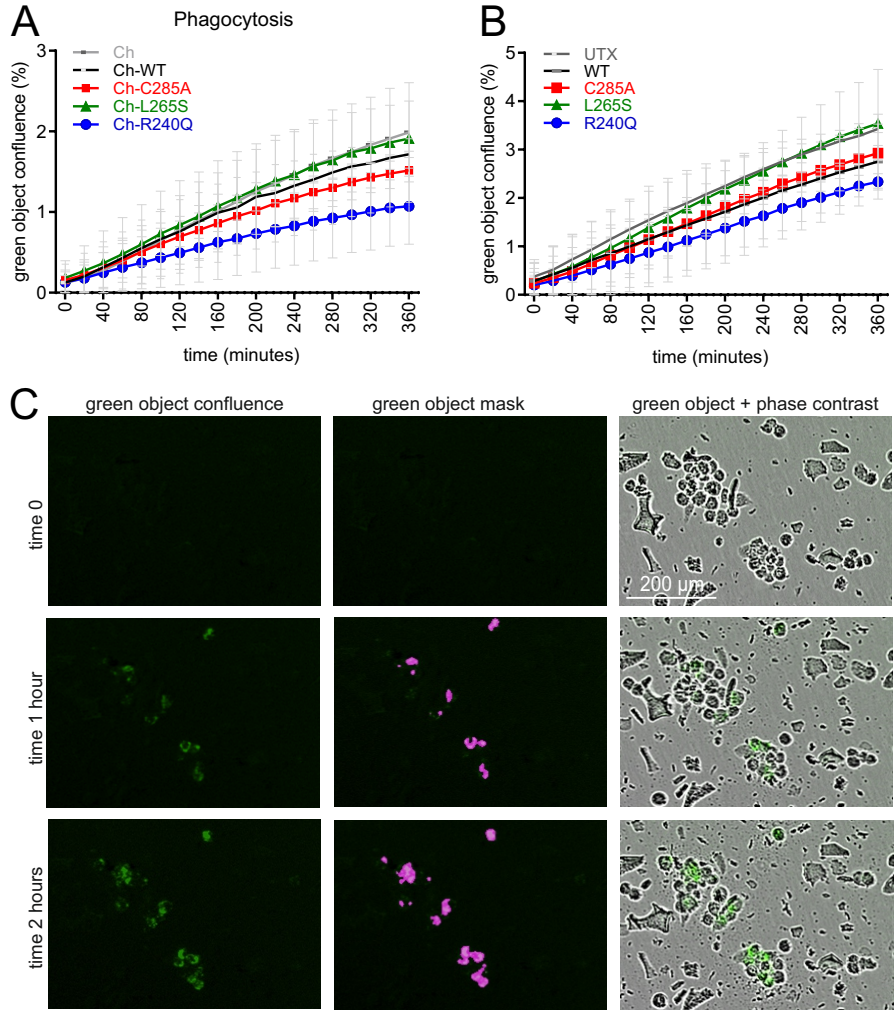
A
Phagocytosis
Ch
Ch-WT
Ch-C285A
Ch-L265S
Ch-R240Q
green object confluence (%)
time (minutes)
B
UTX
WT
C285A
L265S
R240Q
green object confluence (%)
time (minutes)
C
green object confluence
green object mask
green object + phase contrast
time 0
time 1 hour
time 2 hours
200 µm

Figure 4

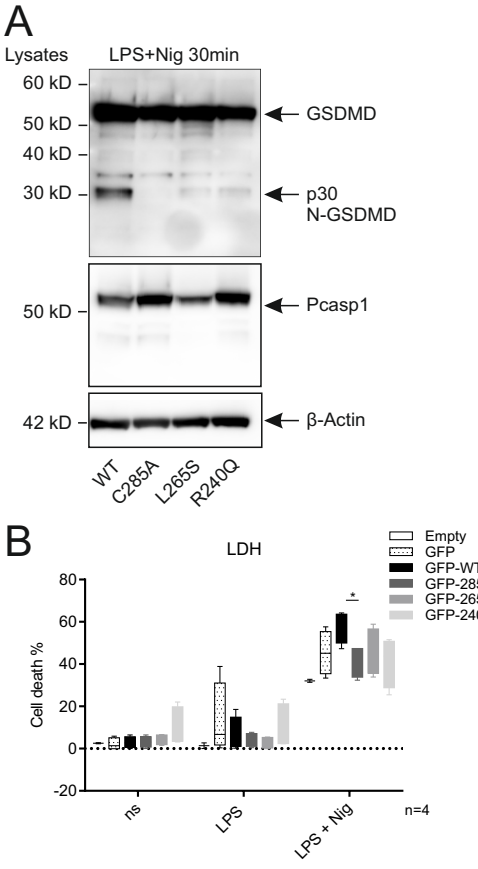
A
Lysates
LPS+Nig 30min
60 kD
50 kD
40 kD
30 kD
GSDMD
p30
N-GSDMD
50 kD
Pcasp1
42 kD
β-Actin
WT
C285A
L265S
R240Q

B
LDH
Empty
GFP
GFP-WT
GFP-285
GFP-265
GFP-240
Cell death %
80
60
40
20
0
-20
*
ns
LPS
LPS + Nig
n=4

Figure 5

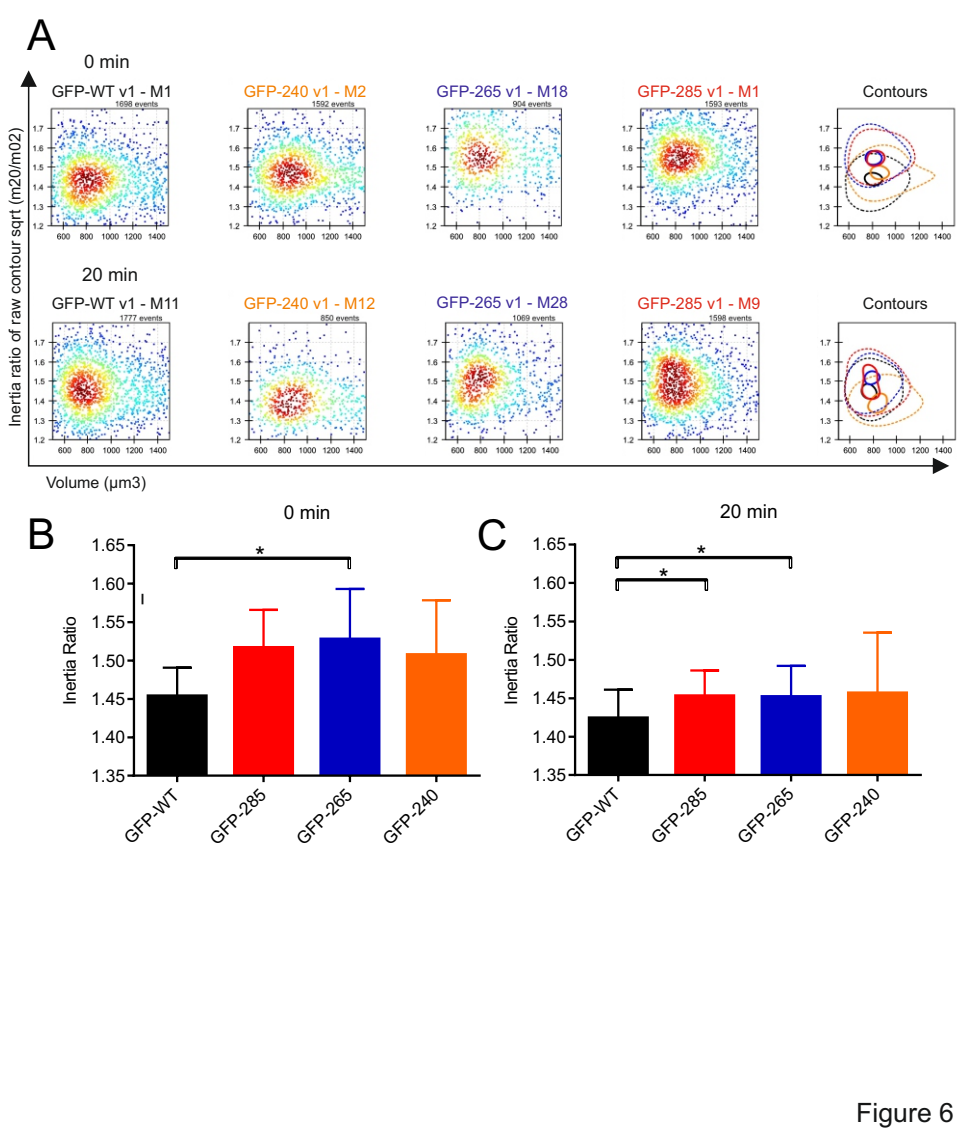
A
0 min
GFP-WT v1 - M1
1698 events
GFP-240 v1 - M2
1592 events
GFP-265 v1 - M18
904 events
GFP-285 v1 - M1
1593 events
Contours
20 min
GFP-WT v1 - M11
1777 events
GFP-240 v1 - M12
850 events
GFP-265 v1 - M28
1069 events
GFP-285 v1 - M9
1598 events
Contours
Inertia ratio of raw contour sqrt (m20/m02)
Volume (µm3)
B
0 min
Inertia Ratio
GFP-WT
GFP-285
GFP-265
GFP-240
C
20 min
Inertia Ratio
GFP-WT
GFP-285
GFP-265
GFP-240

Figure 6

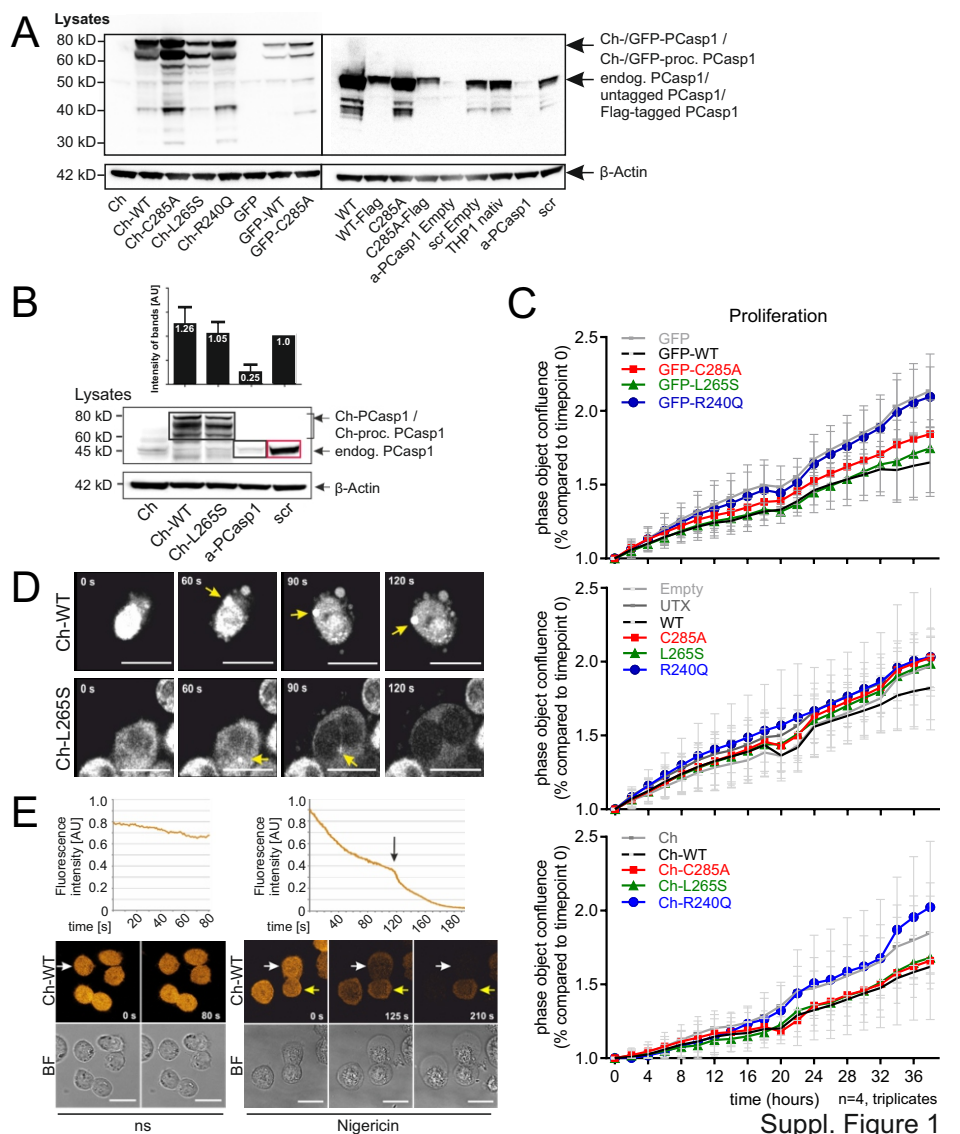

Suppl. Figure 1

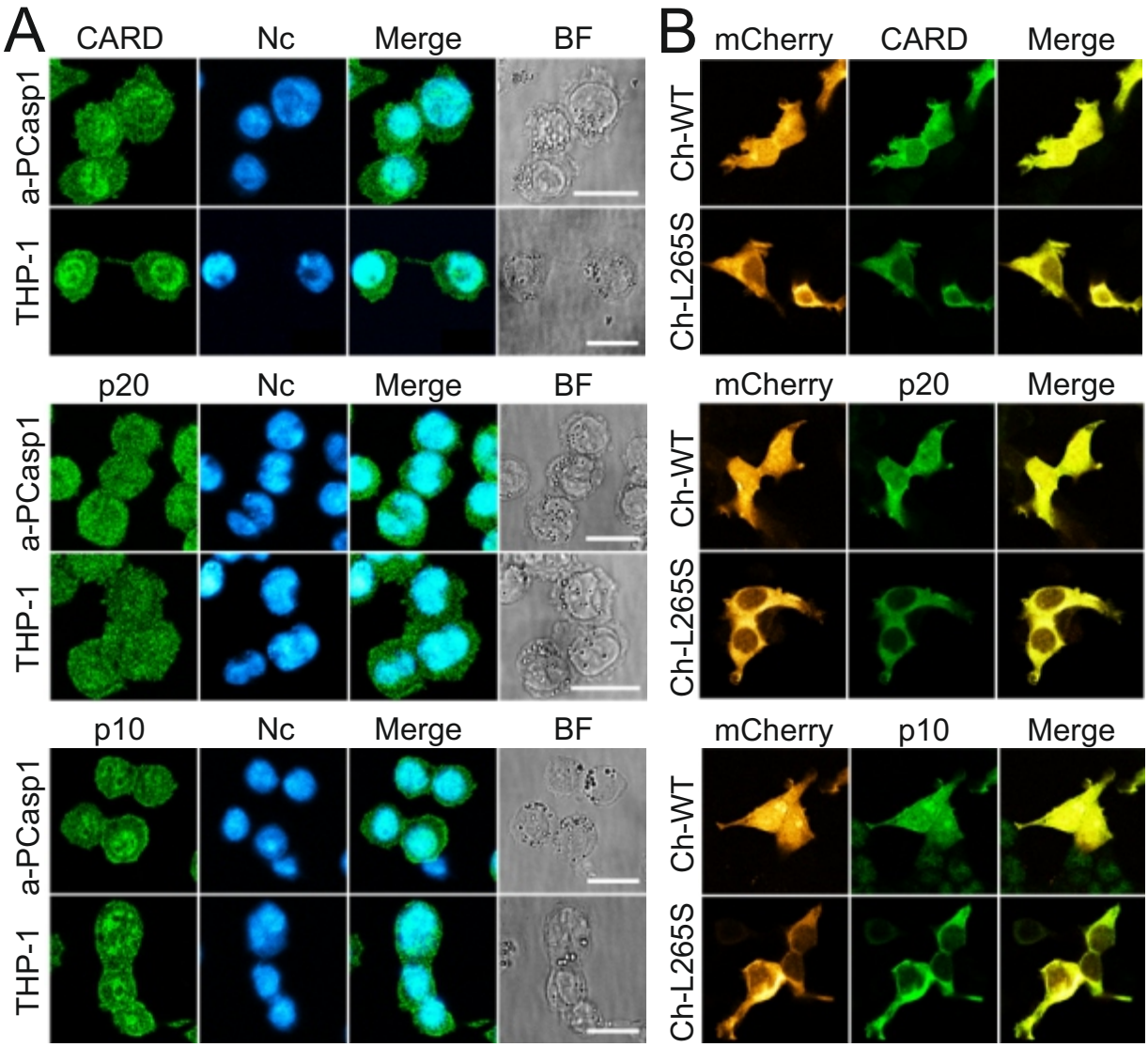

Suppl. Figure 2